EUROPEAN ORGANIZATION FOR NUCLEAR RESEARCH

CERN/ISRC/76-36
ISRC/P95
10 January 1977

PROPOSAL TO THE ISRC

A STUDY OF LARGE-TRANSVERSE MOMENTUM PHENOMENA

CERN[1]-Copenhagen[2]-Lund[3] Collaboration

S. Almehed[3], H. Bøggild[2], E. Dahl-Jensen[2], I. Dahl-Jensen[2],
G. Damgaard[2], G. van Dardel[3], C.W. Fabjan[1], K.H. Hansen[2],
S. Henning[3], G. Jarlskog[3], J.E. Hooper[2], H.B. Jensen[2],
L. Jönsson[3], E. Lohse[2], B. Lörstad[3], R. Møller[2],
S.Ø. Nielsen[2], R. Palmer[1], J.O. Petersen[2],
L. Svenson[3], and W.J. Willis[1]

1. INTRODUCTION

Considerable effort has been devoted in recent years to study high-transverse momentum phenomena in hadron collisions, but many of the most important simple questions remain unanswered. It is the purpose of this experiment to study with the appropriate instrumental techniques those p-p collisions which are characterized by a high transverse momentum flow in the central region. "Jets" should be seen more clearly and their spectrum and associated quantum numbers measured. Larger transverse momenta will be studied, and rare or new particles sought in these events.

Studies to date have been limited by triggers which have been highly biased in favour of events where the energy is concentrated in a single particle. This is clearly the case in experiments triggered by the detection of photons or single charged particles, but it is also true of experiments using a conventional hadron calorimeter, because of the substantially higher response (50%) resulting from electromagnetic showers as compared to charged hadrons.

A new type of hadron calorimeter has been developed at CERN with essentially identical response for charged and neutral mesons and with improved energy resolution[1]. This will allow a satisfactory trigger based on the transverse momentum of a group of particles, independent of the distribution of the energy among the particles and independent of the type of particle. The independence of particle type is subject to an obvious exception related to baryon number, to be discussed later. A single particle calorimeter trigger will also be possible.

The inner detector will allow a trigger on large-p_T charged particles, selecting events (jets), with a well-defined "leading particle". Such events may be important for the understanding of the elementary hard-scattering processes, as, for example, the leading particle is expected to reflect the quantum numbers of the parton producing the jet.

Particle identification in multiparticle events is also essential. In the proposed apparatus, several methods of particle identification are provided, appropriate to different cases. A large fraction of the particles produced within the aperture of the instrument will be identified. With the proposed instrument, it will be possible to investigate a number of questions vital to the understanding of high-transverse momentum phenomena. Among them are:

- the inclusive momentum distribution of jets without bias as to particle distribution within the jet;
- a measurement of the transverse momenta with respect to the jet axis, and of the longitudinal distributions along that axis;
- a study of the momentum and quantum number structure of the event associated with the trigger jet;

- a search for events more complex than two jets;
- the comparison of the production of jets with different quantum numbers carried by the high-p_T particles;
- a comparison between events with a jet trigger and events producing a single particle high-p_T trigger;
- observation of short-lived particles in high-p_T events;
- a search for charmed particles in high-p_T events in decay modes involving strange particles or electrons;
- a search for fractionally charged particles among high-p_T events.

The instrument with which we plan to carry out the research programme includes three parts:

- magnet and inner detector;
- calorimeter;
- Čerenkov counters.

An over-all view is given in Figs. 1a and 1b.

The magnet may be considered as an H-magnet with holes for the beam in the pole pieces. The gap has been opened to provide the greatest angular coverage possible with this type of magnet. The inner detector is cylindrical in form, composed of approximately 50 layers of drift chambers, in which both ionization information and resistive charge division for non-ambiguous two dimensional read-out are available on each wire. This allows good pattern recognition and momentum measurements of good reliability and precision, even for charged and neutral decays inside the chamber. The ionization information allows particles to be identified for P/m less than about 1.5. The relativistic increase in ionization allows electrons to be identified at essentially all momenta, and it may prove useful for pion identification above $\sim$ 3 GeV/c.

The calorimeter is of the fission compensated uranium type, which gives equal response for charged and neutral mesons, measuring the available energy[1]. For mesons, this is the total energy, while for protons it is the total energy less one nucleon mass and for antiprotons, it is total energy plus one nucleon mass. Thus, if a baryon-antibaryon pair enters the calorimeter, the mass terms cancel. For energies above 5 GeV, such a calorimeter has sufficient resolution to give satisfactory results as the principal trigger element, despite the steep fall in the transverse momentum distribution. It includes a front section which is 14 radiation lengths in thickness, to identify the electromagnetic component in the triggering jet.

It is sufficiently finely divided to allow the separation of the energy deposited by different hadrons in most cases, and to make possible the analysis of most multiphoton events.

The Čerenkov counters are envisaged to contain an aerogel radiator covering the range just above that accessible to the ionization measurement, with a threshold around p = 4 m; a gas radiator will count particles above p = 8 m. A third counter at atmospheric pressure can be provided with a threshold around p = 20 m, to complete the pi-K separation for all accessible momenta.

2. PHYSICS PROGRAMME

Inclusive momentum distribution of jets

This is a measurement of the transverse momentum spectrum of "jets". The "jet" refers to a group of particles within a cone of restricted angle, without an implication here that the jet necessarily exists as a distinct physical object. The variables used in describing the jet are shown in Fig. 2. The transverse momentum perpendicular to the vector sum of the momenta of the group of particles must be less than about 0.5 GeV/c for the individual particle to be included in the group.

This measurement must rely on the calorimeter, since neutral particles are usually present, but the momentum measurements in the inner detector are very desirable as a supplementary measurement and control. Most of the neutral energy is probably carried by photons, which are recognized as such in the calorimeter and measured rather accurately. The remaining energy can be compared with the energy carried by charged particles, for each section of the calorimeter, as a check. This leads to the possibility of improved energy resolution as discussed in Section 3.4.

This simple measurement has not yet been performed because of the difficulty of obtaining a calorimeter with adequate resolution, size and unbiased response. The calorimeter proposed here meets these requirements, providing a resolution of about $\delta_E \simeq 0.3 \sqrt{E}$ GeV, adequate for measurement of an invariant cross-section falling as steeply as p^{-8}. The angular range covered is about 90° in θ and 120° in ϕ, referring to Fig. 2. For example, for a jet with p = 6 GeV/c, all particles with fractional momentum $x \geq 0.2$ and $q < 0.5$ GeV/c are contained in the calorimeter aperture if the jet axis lies in a central part of the calorimeter with a solid angle of about 1.3 steradians.

The rate can be estimated roughly by assuming that the rate for π^0 and single photons, which has been measured[2], is about 1/100 of the rate for a jet of the same p_T[3]. An estimate consistent with this prediction is extrapolated from

measurements at p_T of 2 to 3 GeV/c [4]. Then for an integrated luminosity of 10^{36} cm^{-2} (a good ISR day) in a solid angle of one steradian there are $\approx$ 100 expected events with $p_T > 10$ GeV/c.

The rate could be considerably higher if the jet distribution follows the p_T^{-4} distribution predicted by Berman, Bjorken, and Kogut [5] for sufficiently high transverse momenta. This will be one of the first questions studied in this experiment.

Distribution in the jet

For jets of the highest momentum, say $p > 10$ GeV/c, for which there is enough aperture in the calorimeter, the distribution of transverse momentum with respect to the jet axis can be studied, say up to $q = 1$ GeV/c for $x > 0.2$. The x distribution can be studied down to $x \simeq 0.05$. Once the jets are selected by the calorimeter, these measurements rely mainly on momentum determinations in the magnet, though pi-zeros up to several GeV/c and etas over the whole momentum range can be identified in the front section of the calorimeter.

"Multi-jet" events

It may require higher energy storage rings to provide clear examples of multi-jet events, but this apparatus can search for signs that single jet pairs do not explain all high transverse momentum events. This would, for example, involve a search for two jets in the calorimeter. This, indeed, is one of the reasons for making the calorimeter cover such a large range in ϕ.

Quantum numbers in jets

One can never identify with confidence the particles in the jet with small x. If the particles with large x, say $x \gtrsim 0.3$, tend to represent the quantum numbers of the jet in some meaningful sense, their identification will allow the jet to be characterized by charge, flavour, baryon number, etc. In favourable cases, the particles entering the calorimeter can be identified. One may identify protons and antiprotons by comparison of the calorimeter signal with the measured momentum. The short-lived particles are usually identified by analysis of their decays, while the slower particles may be identified by ionization.

However, more effective identification is provided by the Čerenkov counters. The strategy proposed here is to trigger on a high transverse momentum jet in the calorimeter in order to provide, by momentum conservation, a relatively large flux of jets in the direction of the Čerenkov counters. This trigger can be supplemented by use of signals from the inner detector. In this way, a sample of jets of high transverse momentum can be obtained with identification of the charged particles. The layout shown in Fig. 1a and 1b is tailored to such a study.

Correlations of two or more identified High-p_T particles

The trigger for the high-p_T particles will be derived from the inner detector and particle identification provided by two Čerenkov systems on opposite sides. With such a system correlations of quantum numbers of the leading particles in two associated jets will be studied.

Short-lived particles

Charged and neutral decays can take place inside the vacuum chamber or in the detector itself. The latter are clearly more reliably identified and for charged decays particularly, only these are useful. As the jet momentum is increased, decay lengths grow, and a larger fraction of short-lived particles reach the detector. The efficient detection of these decays poses usually a severe problem in pattern recognition, impossible to solve with a small number of position measurements. The generous number of accurate measurements on each track, about 50, reduces the problem of pattern recognition.

Among the known particles we expect to see the strange particles. The inclusive spectrum of K mesons is already known, but their identification provides further information on quantum numbers. It will be interesting, for example, to study the production of hyperons and antihyperons and compare their ratio with those for pairs of ordinary particles. The p_T-dependence for those cross-sections might indicate to what extent high-p_T events are favourable to the search for new particles.

High-p_T events containing charmed particles

The detector has the capability of identifying strange particles ($K^{\pm}$ in the Čerenkov counter and by ionization, and the others by analysis of decays) and electrons (by relativistic rise in ionization). Consequently it is well suited to a search for charmed particles in high-transverse momentum products, where they may be relatively frequent. All the known decay modes are detectable: $K\pi(\pi)$, $K\ e\ \nu$, $\bar{\Lambda}\ 3\pi$. If, for example, a charmed particle candidate is found as the leading particle in the triggering jet, the large solid angle for electron and slow K identification and measurement allows an effective search for the associated particle.

Search for fractionally charged particles

There have been a number of searches for fractionally charged particles at the ISR and elsewhere but none searching with high sensitivity among the products of very high-transverse momentum events. If it is possible to remove a quark from confinement, this would seem to be the way to do it[6].

This apparatus is very powerful as a fractional charge detector because of the large number of samples, combined with good spatial resolution. A few events would already be convincing. The main precaution necessary to carry out this experiment is to ensure that the data handling procedures do not throw out less than minimum ionizing tracks. Since the chamber electronics is designed to deal with the large dynamic range encountered in the charge division technique, it is intrinsically well suited to this problem.

Correlations with the forward cones

The large unobstructed solid angle in the forward cones is a clear advantage of this magnet design. We do not now propose to provide detectors covering this angle, except for some scintillation counter hodoscopes. However, in a later phase it may be attractive to use calorimeters to suppress events where most of the energy goes into the two forward cones.

3. THE APPARATUS

3.1 The magnet

The magnet has been studied extensively, particularly by T. Taylor, ISR. It is a conventional iron-copper magnet, which is completely open and unobstructed over a large range of polar and azimuthal angle. The version shown in the Appendix in Fig. A1 has a free aperture covering $0° < \theta < 15°$, $40° < \theta < 140°$, $165° < \theta < 180°$. The azimuth in these regions is completely open, except for some distant return yokes. The shape of the return yokes is presently being optimized for stray field distribution, accessibility for external detectors and mechanical stability.

The field generated by this magnet is nonuniform as can be seen in Fig. A4, but has of course azimuthal symmetry. (The perturbation of the azimuthal symmetry due to the discrete return yokes is insignificant at the region of the drift chambers.) The choice of the power level at which the magnet will be run, depends on a careful optimization between bending power and acceptable stray fields. It will be in the vicinity of 1 MW.

The field distribution for 1 MW-operation is shown in Fig. A2.

It would be advantageous to thermally stabilize the drift chambers to within $\sim \pm 5°C$. Therefore, thermal shielding of the coils and the use of an auxiliary, heated water circuit whenever the magnet is switched off, may be desirable.

Engineering aspects of the construction of the spectrometer magnet and its associated beam compensating magnets are found in the Appendix.

3.2 The central detector

Scintillators

A cross-section through the central detector is shown in Fig. 3. An inner and outer layer of scintillation hodoscopes, consisting of 44 counters each, cover the full azimuth. Standard timing techniques using commercially available mean timers are used to obtain a timing accuracy of $\sigma \simeq 1.0$ nsec, adequate for the drift chamber strobe. A layer of 8 mm thick scintillators covers completely the vacuum chamber, which is of elliptical cross-section with a length of 150 cm.

Drift chambers

The design of the drift chamber detector is dictated by many requirements of which adequate momentum resolution and optimum layout from the point of view of pattern recognition are the most important. Good momentum resolution is accomplished by measuring typically 45 unambiguous space points along each particle trajectory in the magnetic field.

The second coordinate along each drift wire is obtained by the "charge division" method[7], a technique pioneered and used by the Brookhaven-CERN-Syracuse-Yale Collaboration at the ISR [8,9]. For the detector layout proposed here, the resolution will be $\sigma \sim 0.5\%$ of the wire length. All drift chamber planes are housed in two hemi-cylindrical enclosures to minimize multiple scattering, as shown in Fig. 3. Such a common enclosure also minimizes those systematic errors in the position measurement which depend on gas properties and relative mechanical alignment of the drift cells.

As the "charge division" method requires to measure the charge on the ends of each wire, it is natural to use this information to estimate the most probable energy loss and hence the velocity of each particle. We discuss in Section 3.3 the possibilities for particle identification offered by an ionization measurement with modest accuracy.

Layout of the drift chambers

The multiplicity of the final states we wish to study, the top ISR luminosity, at which the detector is intended to be operated and the multihit-capabilities of the associated electronics determine the solid angle subtended by the drift cells.

Charged particle multiplicities associated with a high-p_T leading particle have been measured by several groups[10]. It is found[11], for example, that in about one steradian cone opposite a 3 GeV/c particle the average charged multiplicity is ~ 1.4, and rising with p_T. If we assume an event with a multiplicity of $\langle n \rangle_{CH} \simeq 20$, we expect double hits in at most 3% of the drift cells in a layout as shown in Fig. 4 and Fig. 5. Note however, that due to magnetic bending the

double-particle overlap will in most cases occur only along a limited segment of the track.

Drift times in the cells limit the event rate and hence the highest luminosity at which the detector can be operated. For our geometry (maximum drift distance 29 mm) and "slow" gases ($v_D \sim 3$ cm/μsec) the drift times will be $\lesssim 900$ nsec, to which a time constant of the electronics of ~ 500 nsec has to be added, giving a total maximum time per event of 1.4 μsec. If one adopts the very conservative attitude to record only those inelastic events which during the sensitive time of the detector were not followed by a second such event, the maximum luminosity is limited to $L < 1 \times 10^{31}$ cm^{-2} s^{-1} with a dead-time not exceeding $\sim 25\%$.

The outer layer (Fig. 5) shows 6 drift wires in a geometry developed by the CHORMN-Collaboration for experiment R606 [12]. In this geometry the direction and position of the track segment is measured without the right-left ambiguity. It is presently being studied whether this information will be useful for the pattern recognition program.

A very last layer of proportional chamber wires is used in conjunction with a cathode strip read-out; this supplements the charge division read-out by providing a further high-accuracy determination of the θ-coordinate ($\sigma < 1$ mm expected). We intend to introduce two or three further layers of proportional wires, which will provide a fast logic trigger on high-p_T charged particles formed by hardware coincidences in radial sectors.

The drift chamber parameters are summarized in Table 1.

Table 1

Drift chamber parameters

Layer	Radius at first sense wires [mm]	Radius at last sense wires [mm]	Drift gap [mm]	Number of sense wires
I	204	316	8-11	1350
II	424	576	15-20	1800
III	722	825	25-29	1440

The distribution of the electric drift field has been calculated [13] for an approximate geometry and is shown in Fig. 6. It is very uniform to within a very small distance from the sense wires.

Momentum resolution

Gluckstern[14] has shown that N measurements along the length L of a track segment minimize the effect of measurement errors, if these N measurements are grouped as N/4 at L = 0, N/2 at L = 1/2 and N/4 at L. Our detector layout (Fig. 3) reflects this optimization prescription. The calculated resolution for such a layout is computed in Table 2 assuming a drift chamber resolution of σ = 200 μ. Note that these figures assume only half the possible improvement in curvature measurement when going from an evenly distributed to a totally lumped layout, an assumption which should reasonably well reflect the actual layout.

Table 2

Momentum resolution

	$\Delta p/p^2$ [GeV/c^{-1}] due to measurement error (σ = 200 μm)		$\Delta p/p$ due to multiple scattering for β = 1 particles (1 MW)	
	0.65 MW	1.0 MW	Xe/CO_2	A
90°	1.46×10^{-2}	1.24×10^{-2}	2.5×10^{-2}	1.3×10^{-2}
70°	1.31×10^{-2}	1.13×10^{-2}	2.5×10^{-2}	1.3×10^{-2}
50°	0.81×10^{-2}	0.70×10^{-2}	2.2×10^{-2}	1.1×10^{-2}

The contribution due to multiple scattering of the material in the detector and for two different gas fillings are also given in Table 2; over-all resolution is shown in Fig. 7 for two different particle directions. It demonstrates a favourable property of this detector: the resolution at intermediate angles is higher compared to the 90° direction. Reasonable momentum resolution exists even for more forward particles. A particle emitted, for example, under an angle of 55° with respect to 90° will be measured with an accuracy of $\Delta p/p^2 \sim 0.02$ GeV/c^{-1}.

The detailed layout of the drift chambers will also depend on aspects of pattern recognition and is presently being finalized. However, the power of this detector with regard to pattern recognition can be appreciated from Figs. 8-10, showing the tracks of Monte Carlo generated events.

Drift chamber operation in inhomogeneous magnetic fields

These drift chambers have to operate in inhomogeneous magnetic fields. The standard procedure of compensating with an appropriately tilted electrical drift field is not practical. Measurements[15] have shown that the drift velocity itself is not affected even by very high magnetic fields (up to 1.9 T). We therefore have to consider only the ratio of the magnetic to electric forces $R = (B \cdot v_D)/E_D$;

at a given magnetic field this ratio can be minimized by choosing a gas, which in the saturated drift region has a low drift velocity and by increasing E_D to the highest practical values. We intend to take both steps: one gas we consider is 80% Xe/20% CO_2 mixture, known to be an excellent MWPC gas with excellent stability and high gain[9]. Its drift velocity is $v_D \sim 3$ cm/μsec. Another gas we intend to investigate is neopentane, which offers advantages of reduced multiple scattering and dE/dx fluctuations. The small drift gaps we intend to use favour the practical use of high drift fields. A value of $E_D = 3$ kV/cm appears possible. Measurements on the apparent change in drift velocity[16] have been extrapolated to our case

Table 3

Software corrections for drift chambers in a magnetic field

Magnetic field	Type of correction	Magnitude of correction
Zero	Inclined tracks	For 30°, $\Delta \simeq 0.9$ mm For 45°, $\Delta \simeq 1.4$ mm (∿ two iterations required)
	Signal propagation along wire	∿ 150 μm/m of wire
	Tracks close to sense wires	Depends on distance from sense wire
Homogeneous field	Tilt angle α $\alpha = \tan^{-1} \frac{B \cdot v_D}{E_D}$	If not compensated the apparent change in v_D is: 0.2% at 0.10 T 2.5% at 0.30 T 12 % at 0.60 T for "standard" operating conditions
Inhomogeneous as in the "open axial field magnet"	Apparent change in v_D	Possibilities for hardware correction: i) increase drift field to highest practical values ii) decrease drift velocity Magnitude depends on $B \cdot v_D / E_D$ See Fig. 11 for numerical values.

and are shown in Fig. 11. We see that the effect of the magnetic field is small and can be treated in software on the same scale as other corrections, which have to be considered in software for normal drift chamber operation, as listed in Table 3. However, the full measurement accuracy and hence these extensive corrections are only necessary for the few high-p_T particles in an event.

3.3 Particle identification

Multiple ionization measurements

Increasingly, particle identification based on multiple ionization measurements of the relativistic rise is being used for highly relativistic particles[17]. However, we see as the most useful application of these techniques to ISR-physics in the central region the identification of particles with velocities less than minimum ionizing, which constitute a large fraction of the centrally produced charged particles. This identification requires only moderate resolution and permits therefore identification over very large solid angles.

The prediction for our detector and gas mixture (80% Xe/20% CO_2) are based on two recent measurements[17,18], using different A-gas mixtures. Furthermore, these measurements are consistent with recent refined calculations on the relativistic rise and the Landau width of the dE/dx loss in thin samples[19]. From these publications one obtains information on the energy loss and Landau width for a 80% Xe/20% CO_2 mixture, which is consistent with the measurements of the R806 group[9] (FWHM in 1 cm Xe/CO_2 = 90%). This suggests that in one 8 mm gap of our drift chambers a Landau width of FWHM = 100% will be observed, identical to the resolution measured in a 15 mm sample of A/CH_4 [18]. Global resolution found for 58 samples was FWHM = 13%, which contained however, a 5.5% cross-talk contribution due to electronics and δ-rays. A similar result, FWHM = 14%, is obtained by extrapolating the optimization procedure given by Aderholz et al.[17]. Consequently, we expect that a resolution figure of FWHM = 15% is achievable in a set-up of simple geometry but otherwise with parameters identical to our chambers. However, future tests will have to demonstrate whether in our detector geometry a resolution can be achieved which would allow us to separate pions from kaons and protons on the relativistic rise.

Figure 12, which was prepared using the data of Ref. 19, shows that considerably coarser resolution is adequate for particles with velocities below minimum ionizing. The range of momenta of π's, K's and p's, which can be identified in our detector is given in the first column of Table 4. More than 80% of all centrally produced charged particles can be identified with this method alone.

Table 4

Particle identification

Particle \ Method	I $\frac{dE}{dx} \propto \frac{1}{\beta^2}$ regime	II Aerogel Č $\gamma_{th} = 4.2$	III Pressure Č $\gamma_{th} = 8.2$	I + II + III	IV Relativistic rise of dE/dx	I + II + III + IV
π	0.06-0.8 GeV/c	0.6-2.1	1.1-4.0	0.06-4.0	3.0 →	0.06 →
K	0.1 -0.8 GeV/c			0.1 -1.2 and 2.1 -4.0		0.1 -1.2 and 2.1 -7.7
p	0.1 -1.2 GeV/c	2.1-4.0	4.0-7.7	0.1 -1.2 and 2.1 -7.7		0.1 -1.2 and 2.1 -7.7
e					0.2-5.0 *)	

*) Electrons of these momenta saturate the relativistic rise and are therefore distinguishable from the hadrons even with moderate resolution of the ionization measurement.

External Čerenkov counters

Identification of high momentum particles will be achieved by the use of two layers of Čerenkov counters, of large solid angle. For the inner counter of refractive index of about 1.03 (corresponding to a threshold of 0.6 GeV for pions, 2.1 GeV for kaons and 4.0 GeV for protons), we intend to use an aerogel radiator. This type of material has only been used up to now for test purposes but not in an actual experiment. However, progress made up to now in Saclay, DESY and Lund indicates that this technique could be available for use with the proposed experiment. Further development work and mass production facilities are required, to which our collaboration is prepared to contribute. In Lund test pieces of aerogel of good optical quality have been manufactured and active considerations of the large scale production has been started.

The outer Čerenkov counter with a refractive index of about 1.0075 will use as a radiator Neopentane at a pressure of $\sim$ 3.5 atm. We are presently investigating several design options, among them a modular concept, where the radiator is contained in several thin-walled enclosures.

A possible schematic layout is shown in Fig. 1a and 1b. We do not anticipate any problems with stray magnetic fields on the photomultipliers: at their position the field is at a level of $\sim$ few hundred gauss, adequately low for conventional shielding techniques. A summary of the possible particle identification is given in Table 4.

3.4 The calorimeter

The detector is subject to the following requirements:

i) To register the energy distributed over a jet without bias as to the number of constituents, or fraction of electromagnetic energy.

ii) To provide sufficient resolution, particularly in regard to a sharp cut-off on the upper end of the response curve, to give a meaningful trigger for very large transverse momentum.

iii) To distinguish electromagnetic showers from those initiated by hadrons.

iv) To provide sufficiently fine grained unambiguous subdivision that showers from individual particles can be resolved with a small fraction of overlap.

v) To cover the whole polar angle left free by the magnet, $\sim 90^\circ$, and an azimuthal angle of 120°, large enough to allow the observation of "multi-jet" events.

The first requirement is met by the use of a fission-compensated calorimeter of uranium, as explained in detail in Ref. 1.

The resolution also depends crucially on the compensation of nuclear effects: otherwise the fluctuations in the fraction of electromagnetic energy within individual hadronic showers dominates the energy resolution. It is also necessary to suppress sampling fluctuation by the use of thin plates. It was shown in Ref. 1 that the use of 1.7 mm plates in liquid argon provided a resolution of 10% standard deviation at 10 GeV, substantially limited by sampling fluctuations. Here we plan to use 1.5 mm uranium plates. It was found[1)] that a sufficiently deep calorimeter gave a Gaussian response. In the present case we are more concerned with the shape of the resolution curve on its upper side, because of the steeply falling distribution in transverse momentum. A small tail on the lower side of the resolution function becomes unimportant when convoluted with the momentum distribution. We have studied the shape of the resolution function obtained in Ref. 1 for absorbers of different depths, and have found that satisfactory results are obtained for a calorimeter of 210-1.5 mm uranium plates, about five interaction lengths. The response function when folded with the transverse momentum spectrum is shown in Fig. 13.

The electromagnetic and hadronic showers are distinguished by the separate read-out of the first 14 radiation lengths of the absorber, about 0.3 interaction lengths. Charged hadrons, which have a momentum determined by the inner detector, are rejected by a factor of several hundred by a comparison with the calorimeter response. Neutral hadrons are rejected by a factor of about fifty on the basis of calorimeter signals alone.

The fourth requirement specifies that the showers be separated unambiguously. Given the concentration and multiplicity of particles in high energy jets, we believe that reconstruction by stereoscopic views with strip read-out is unsuitable. Accordingly, the calorimeter is divided into square blocks subtending $5^\circ \times 5^\circ$, and each of these is read out separately. Each block is divided into two sections longitudinally, as described in the previous paragraph.

The cell size of 5° may be justified by estimating the overlap. Because of the longitudinal separation, the electromagnetic and hadronic showers are effectively separated. Furthermore, if two charged tracks fall in the same cell it does not matter, since their momentum will have been measured in the inner detector. Thus the neutral hadrons (n, $\bar{n}$, K^0, $\bar{K}^0$) form the class of particles critical for the overlap considerations. We take as an example a 10 GeV jet with four charged hadrons, four distinct photon showers, and one neutral hadron, distributed over about 40 cells. The probability that the neutral hadron coincides with one of the others, including the photons, is about 20%. The overlap is certainly not negligible, but it is clear that the majority of neutral hadrons will be clearly distinguished, so that it should be possible to estimate the number which do overlap.

It is not easy to reduce the cell size a great deal. If the calorimeter cell is made up of 1.5 mm uranium and 2.5 mm liquid argon, the 5° cell has a diameter of about one interaction length, if the calorimeter starts at 1.3 m from the source. Then about 70% of the energy from a hadron shower is deposited in one cell, and it is not profitable to make it smaller. Moving the calorimeter further from the source makes it more massive and expensive.

The 5° cell allows pi-zero reconstruction for momenta up to $\sim$ 1.5 GeV, and eta reconstruction up to $\sim$ 5 GeV. This could be improved, but at the cost of more read out, and it does not seem necessary for the purposes now envisaged. If fine angular resolution is required, the detector of R806 could be used.

Use will be made of this spatial resolution of the showers when evaluating the total energy of the jet. The energy due to charged hadrons, about half the total energy, will be determined by the inner detector with a resolution of $\sim$ 3-10%, or better if the calorimeter is used in the energy measurement. The photons, carrying about 30% of the energy, will be measured with a resolution of about 5%.

The neutral hadrons, carrying perhaps 20% of the energy, will be measured with a resolution of $\sim$ 20%. Thus the over-all energy resolution should be better than 5%.

The number of cells required is 486, with 972 read-outs, half of which now exist in R806. It is envisioned to place the stacks of plates in a cellular structure of aluminium plates with a mass of less than one ton, giving a small percentage of dead volume. The liquid argon tank will be insulated with Perlite, and will have an internal heat exchanger, giving a simple and efficient cryogenic system.

4. RESPONSIBILITIES AND SCHEDULES

We expect CERN to take the responsibility for the magnet and the drift chamber detector. We also need CERN software support in collaboration with the Scandinavian participants for the optimization of the inner detector.

Responsibility for the particle identification system and scintillators is taken by the Scandinavian Groups. Development of the Pattern Recognition Programs will be a Scandinavian activity, centred in Copenhagen. For the geometry programs CERN help may be asked. The Scandinavian groups, in collaboration with the EPDH-Group, will be responsible for the on-line software.

We expect that the responsibility for the calorimeter will be divided between CERN and another collaborator, whose participation cannot yet be confirmed.

Table 5

Major construction and electronics items

Item	Cost [kSFr]	Comment
Magnet	1,300	
Drift chambers (DC)	400	
DC - gas system	100	
Particle identification	1,000	
Calorimeter		
Cryostat	200	
60 tons U238	400	Cost for machining; we have offers for the loan of the material
Cryogenics	-	exists in R806
5,000 channels of drift time digitizers	750	Without preampl. + cables
Linear drift chamber El.	1,200	(ADC's and shaping amplifiers)
500 channels of Calor. El.	150	(500 channels exist already in R806)
DC - preampl.	130	
Fast electronics for particle ident. and scint.	(500)	Exists in the Scand. Groups
CAMAC crates	200	
MIN + CAMAC electronics		Partly existing in R806

Cost estimates for the major components are given in Table 5. Engineering estimates indicate that the equipment will be ready for installation in the winter shutdown 1978-1979, assuming an early approval.

The great flexibility offered by our experimental approach suggests several experimental phases, with different layouts of the external detectors. We consider the running of the various phases to be a matter of scheduling.

We wish to thank P. Innocenti, A. Rothenberg, and F. Sauli for help.

REFERENCES

1) C.W. Fabjan, W. Struczinski, W.J. Willis, C. Kourkoumelis, A.J. Lankford and P. Rehak, Nuclear Instrum. Methods (to be published).

2) F.W. Busser et al., Phys. Letters 46B, 471 (1973).

3) M. Jacob and P. Landshoff, CERN preprint TH.2182.

4) British-French-Scandinavian Collaboration, ISR experiment R413, preliminary data,

5) S. Berman, J. Bjorken and J.B. Kogut, Phys. Rev. D 4, 3388 (1971).

6) See, for example, L.G. Landsberg, Report IFVE 73-48 (1973).

7) V. Radeka, IEEE Trans. Nuclear Sci. NS-21, 51 (1974).

8) J. Fischer et al., Nuclear Instrum. Methods,

9) J. Cobb et al., Nuclear Instrum. Methods, to be published.

10) For a recent review see, for example, P. Darriulat, Rapporteur's talk, 8th Internat. Conf. on High-Energy Physics, Tbilisi, 1976 (to be published).

11) British-French-Scandinavian Collaboration, ISR experiment R413, preliminary data.

12) C. Rubbia and D. Schinzel, private communication.

13) A. Rothenberg kindly provided the program for these calculations.

14) R.L. Gluckstern, Nuclear Instrum. Methods 24, 381 (1963).

15) A. Breskin et al., Nuclear Instrum. Methods 124, 189 (1975).

16) A. Breskin et al., Nuclear Instrum. Methods, 119, 9 (1974).

17) M. Aderholz et al., Nuclear Instrum. Methods, 118, 419 (1974).

18) W.L. Allison et al., Nuclear Instrum. Methods, 133, 325 (1976).

19) J.H. Cobb et al., Nuclear Instrum. Methods, 133, 315 (1976).

Figure captions

Fig. 1 : a) Over-all view of the experimental apparatus in the plane normal to the beams.
b) Over-all view of the experimental apparatus in the plane of the beams.

Fig. 2 : Coordinate system and nomenclature used in the description of jets. The jet axis is defined by the total momentum vector $\vec{p}$ of the particles in the jet, having momenta $\vec{p}_i$. The component of $\vec{p}$ along the x-axis gives p_T of the jet, while the transverse momenta of the $\vec{p}_i$ with respect to $\vec{p}$ are designated q. The fractional momentum of a p_i along the jet axis is called x, in units of $|\vec{p}|$.

Fig. 3 : Cross-section through the central detector.

Fig. 4 : Detail of the inner 15 drift chamber planes.

Fig. 5 : Detail of the outer 16 drift chamber planes.

Fig. 6 : Equipotential lines of the drift field. The slight radial increase of the drift field will be compensated with the appropriately stepped cathode potential applied to the strip cathodes, which run parallel to the sense wires.

Fig. 7 : Momentum resolution obtainable with the detector with the magnet operated at 1 MW. The effect on multiple scattering of different gas fillings are shown.

Fig. 8 : A three dimensional view of a typical event in our detector. The symbols along a track indicate the hits in the drift chambers.

Fig. 9 : The same event projected into the r-ϕ plane. ϕ is the azimuthal angle.

Fig. 10 : The same event projects into the r-Z plane.

Fig. 11 : Apparent change in drift velocity as a function of magnetic field. A drift velocity of v_D = 3 cm/μsec and a drift gap of 20 mm is assumed, while two values of the drift field E, are shown. This figure represents an extrapolation of measurements reported in Ref. 16.

Fig. 12 : Most probable energy loss of π's, K's, p's and electrons in 8 mm of 80% Xe/20% CO_2.

Fig. 13 : a) Trigger efficiency of the calorimeter when set to a nominal threshold of 5 GeV (dashed line). The solid line shows the true energy (p_T) spectrum of events accepted by this calorimeter setting, assuming a p_T-dependence for those events similar to the inclusive π^+-spectrum.

b) Same as (a) but smearing of trigger threshold due to two additional low energy particles. About 30% of all triggers will have a particle with E > 5 GeV.

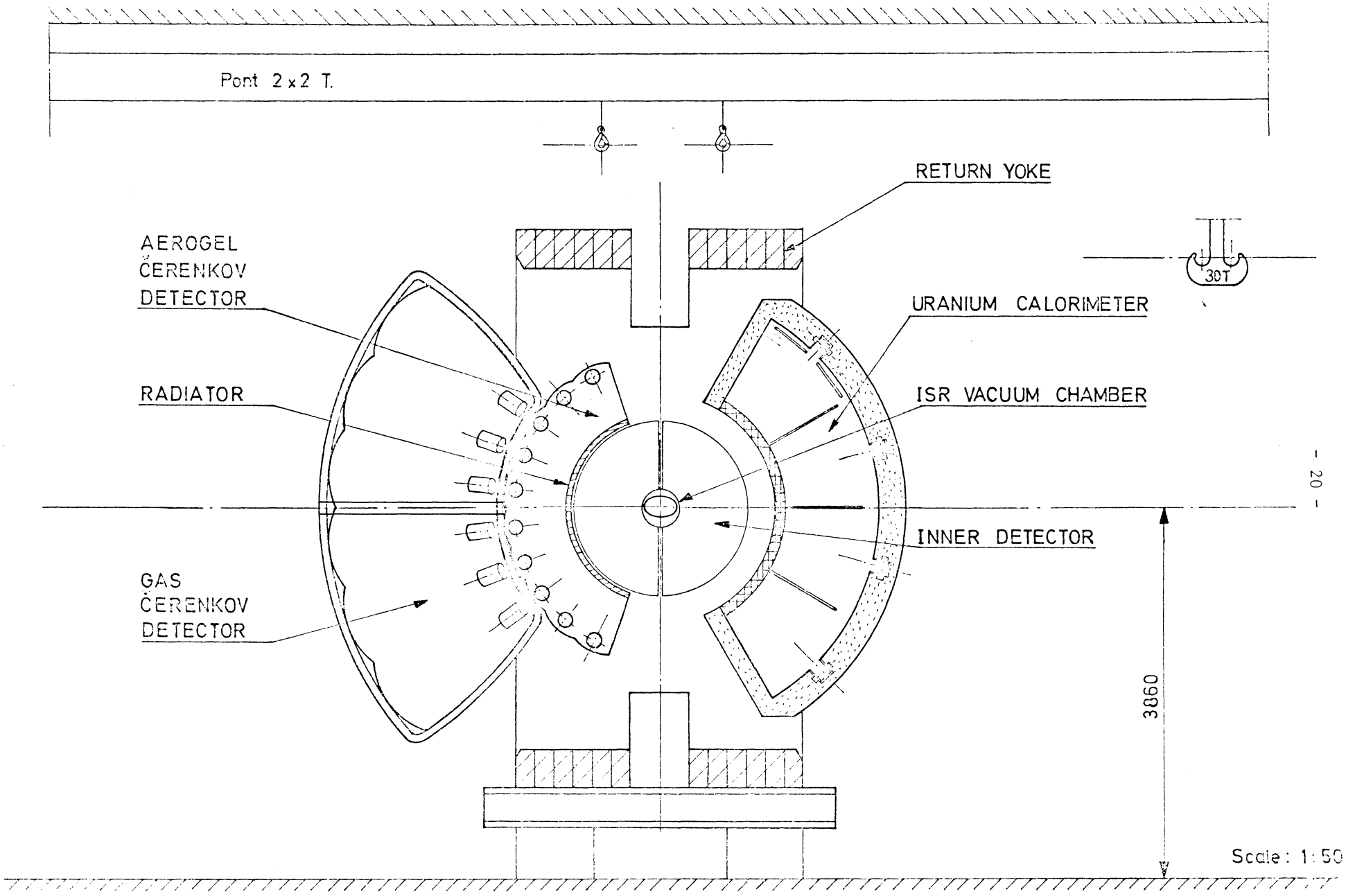

Fig. 1 (a) Cross-section showing outer detectors

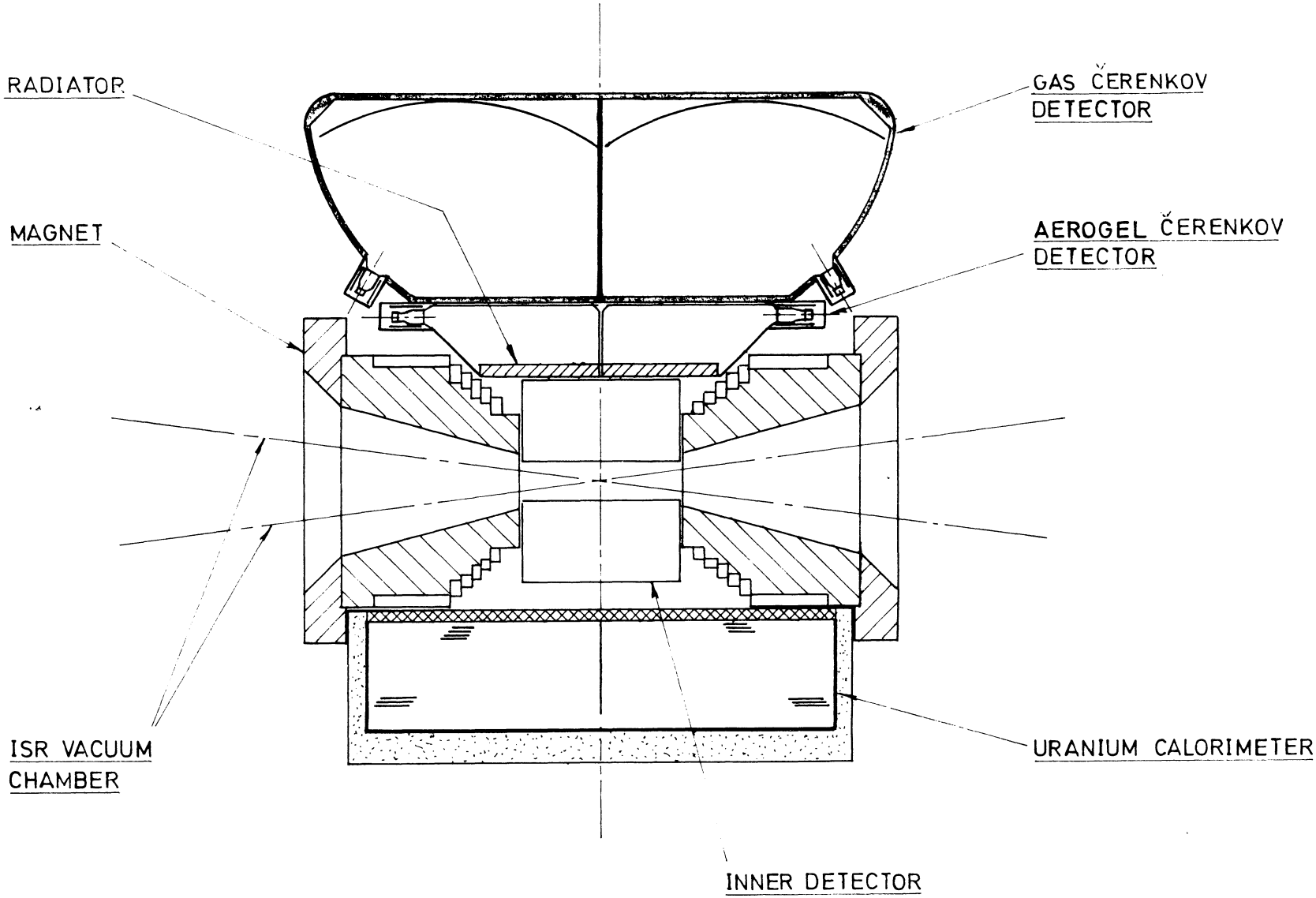

Scale 1:50

Fig. 1 (b) Plan section showing outer detectors

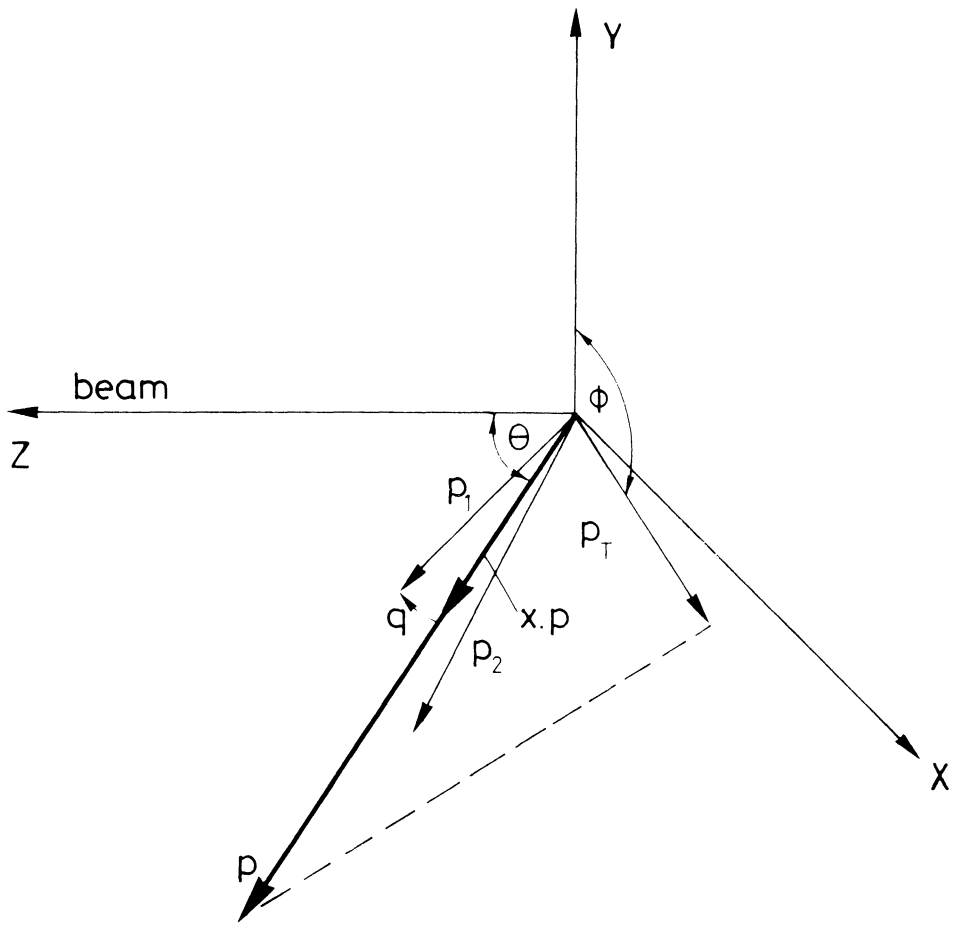

Fig. 2

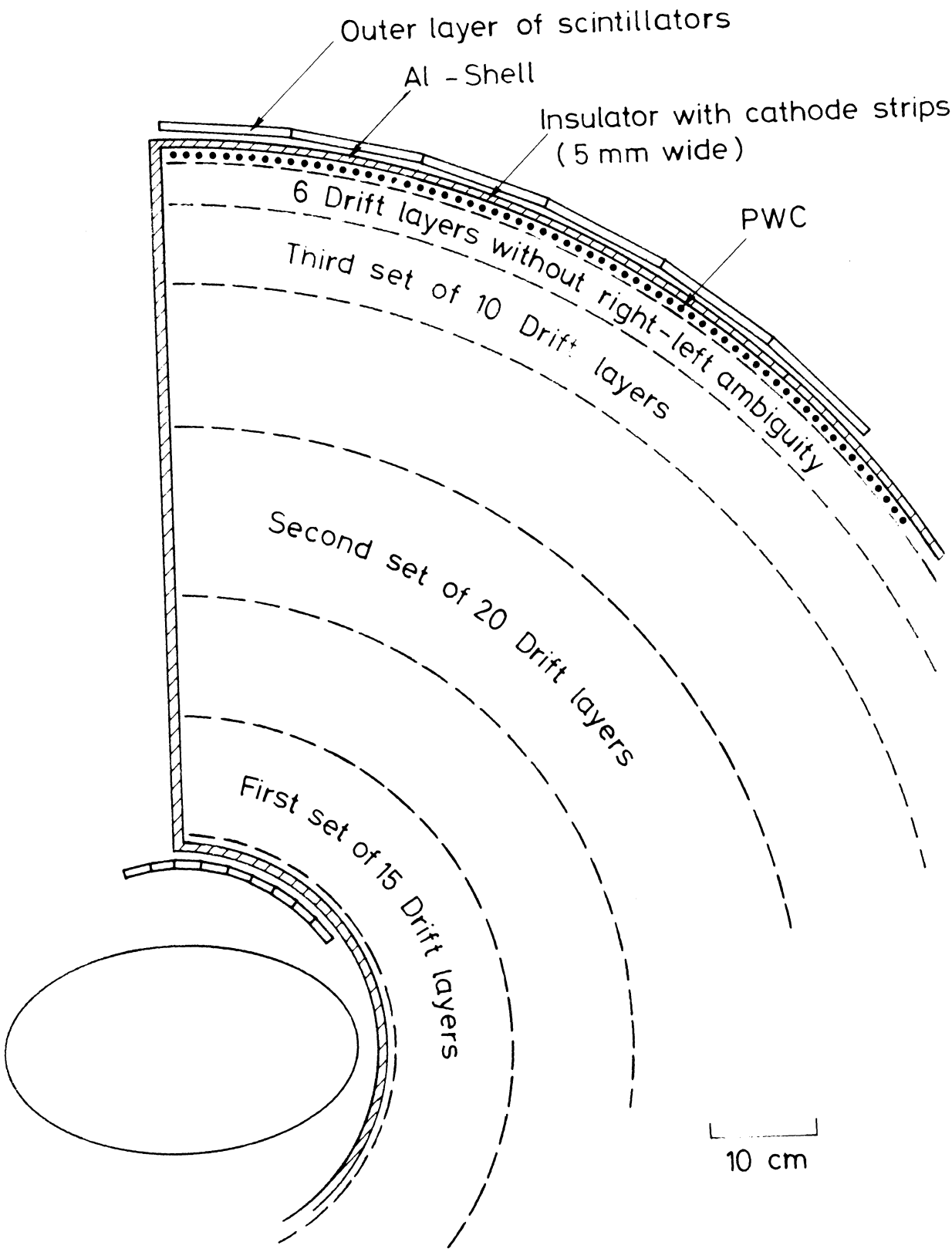
Outer layer of scintillators
Al - Shell
Insulator with cathode strips
(5 mm wide)
PWC
6 Drift layers without right-left ambiguity
Third set of 10 Drift layers
Second set of 20 Drift layers
First set of 15 Drift layers
10 cm

Fig. 3

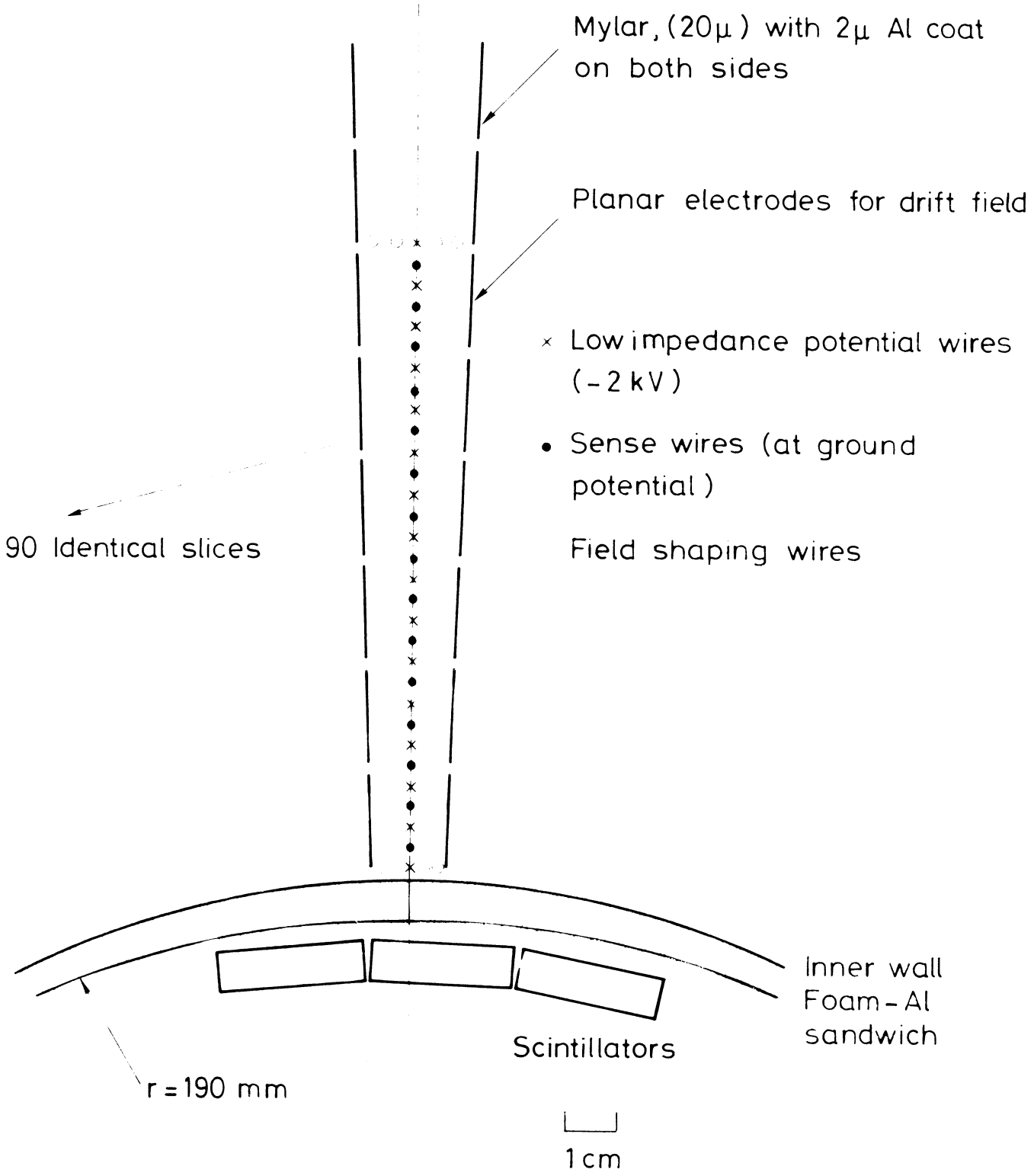
Mylar, (20μ) with 2μ Al coat on both sides
Planar electrodes for drift field
× Low impedance potential wires (-2 kV)
• Sense wires (at ground potential)
Field shaping wires
90 Identical slices
Inner wall Foam-Al sandwich
Scintillators
r = 190 mm
1 cm

Fig. 4

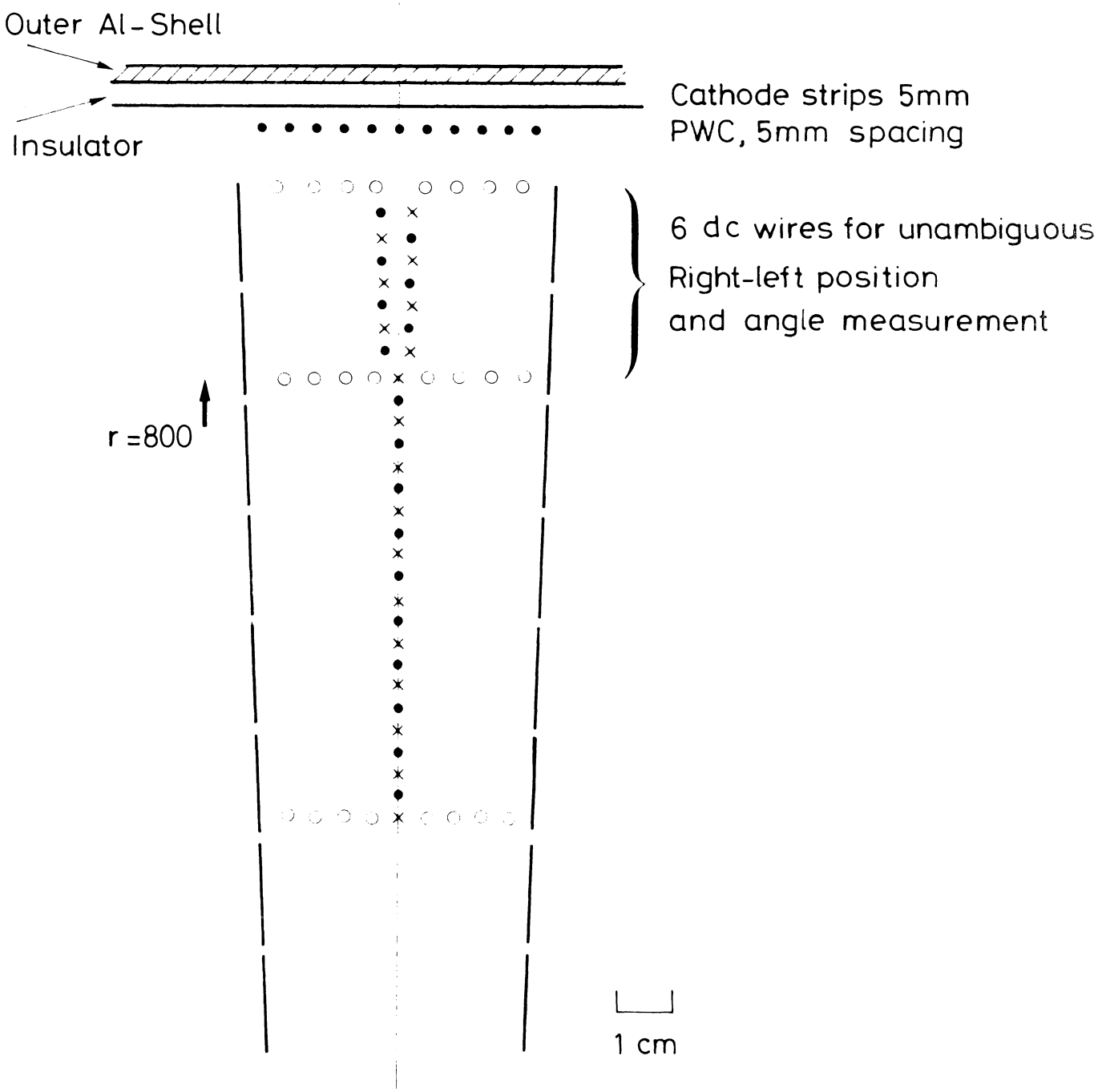
Outer Al-Shell
Insulator
Cathode strips 5mm
PWC, 5mm spacing
6 dc wires for unambiguous
Right-left position
and angle measurement
r =800
1 cm

Fig. 5

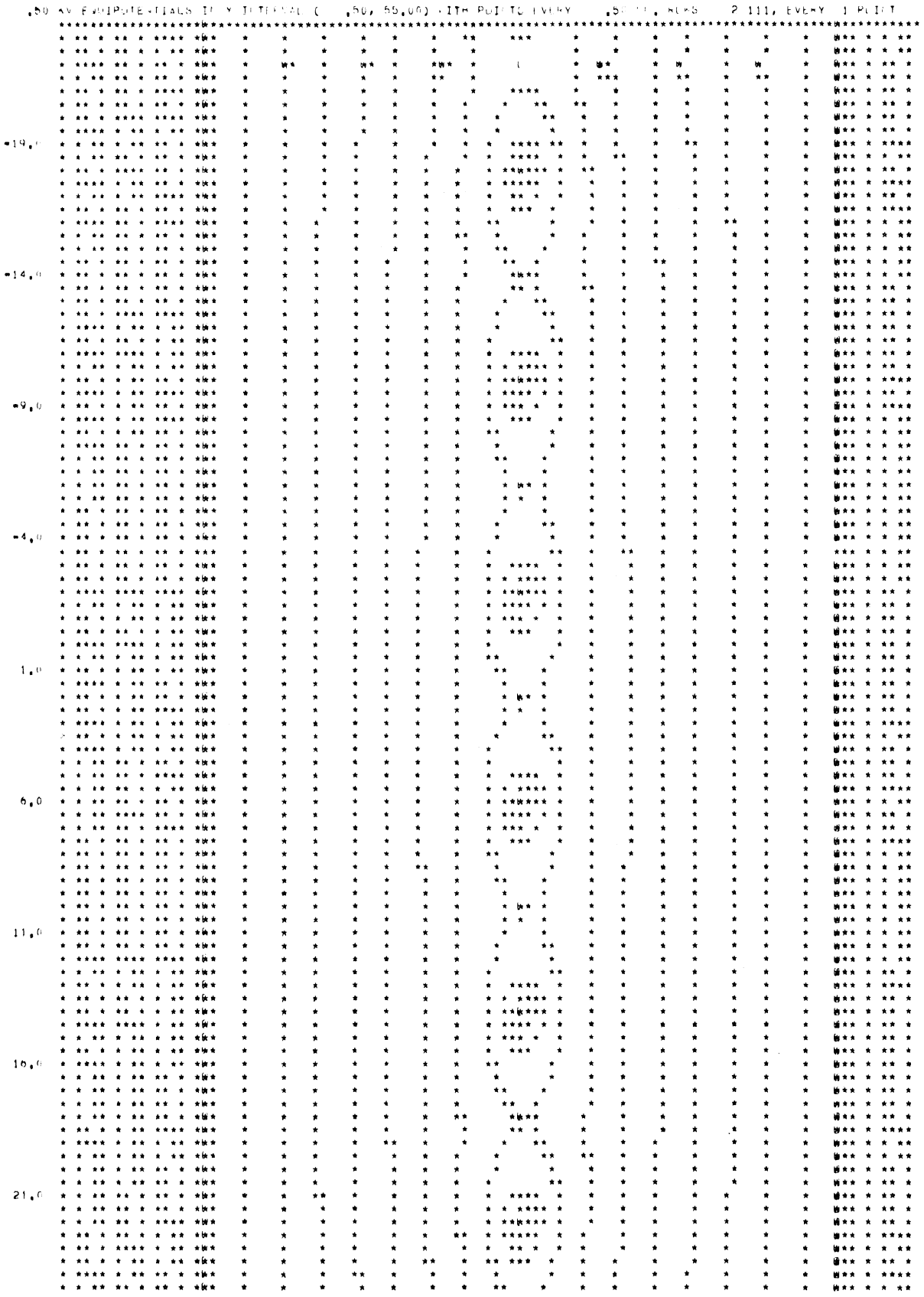

Fig. 6

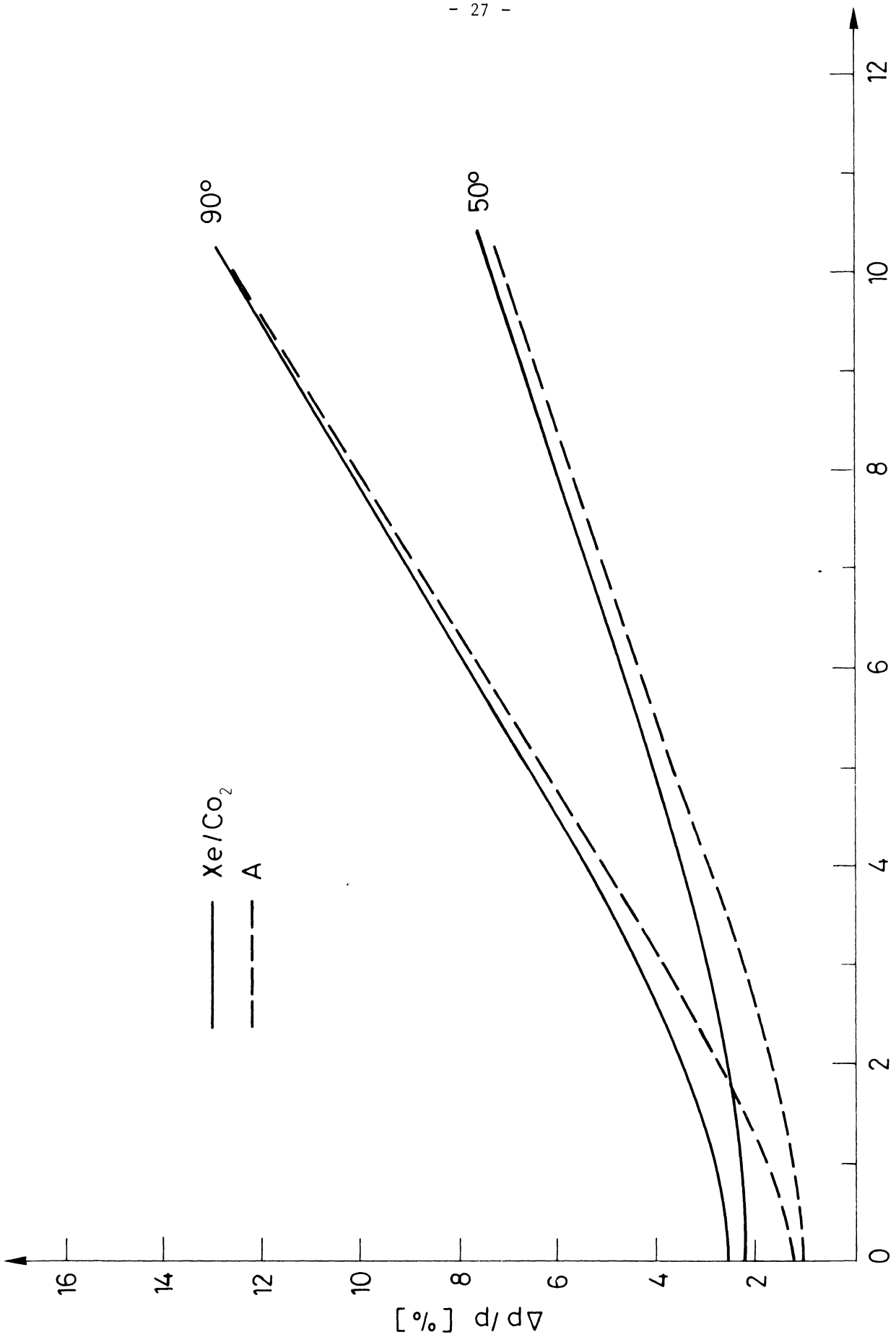

Fig. 7

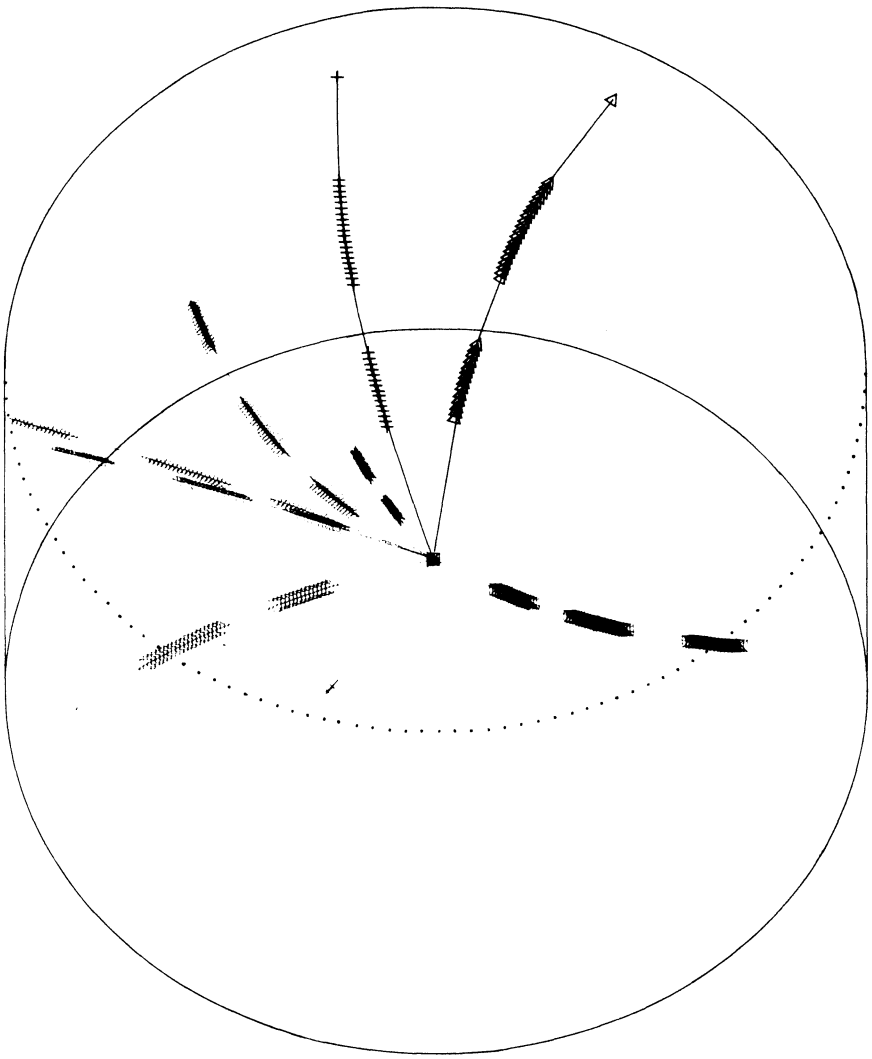

Fig. 8

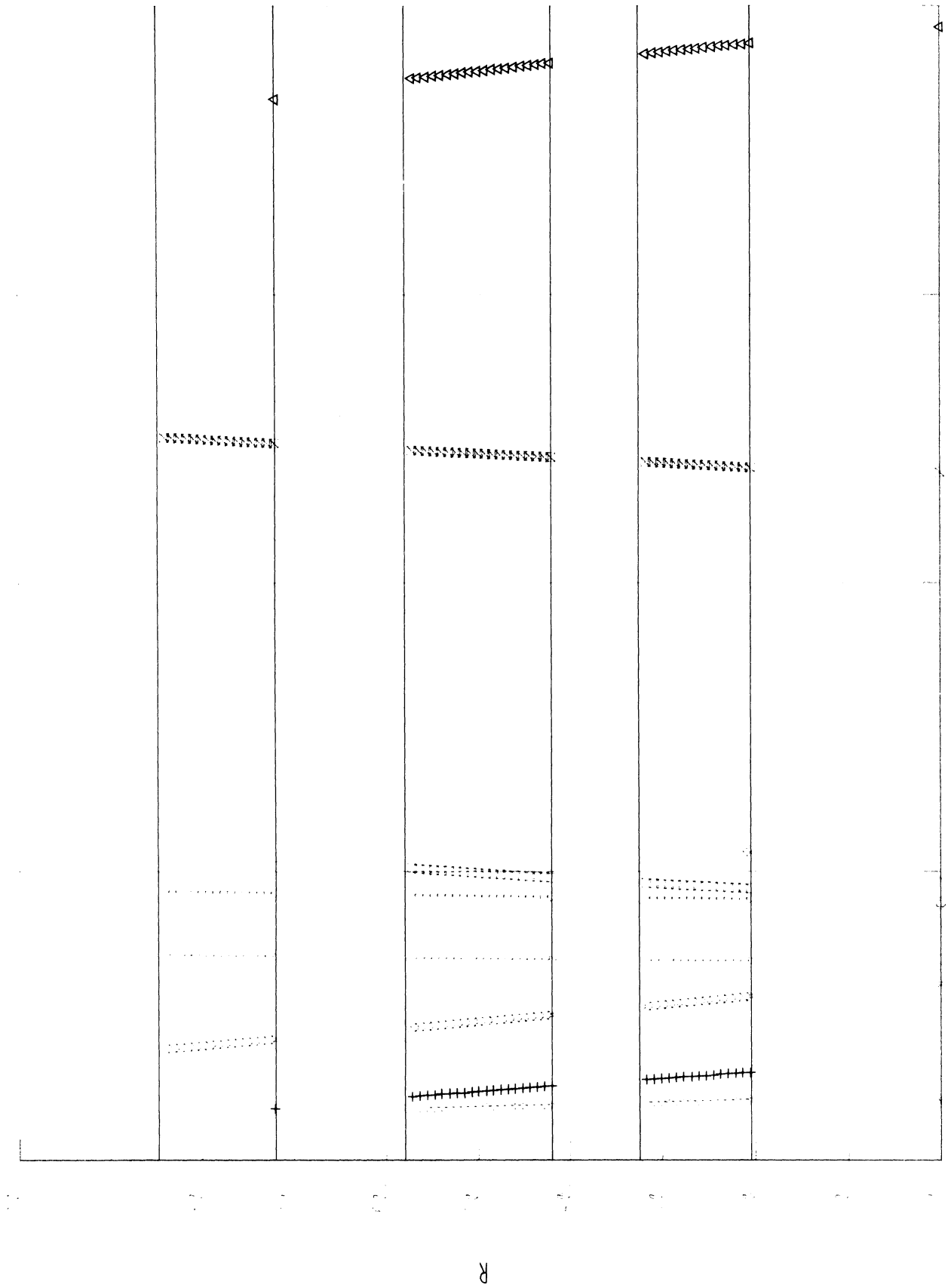

Fig. 9

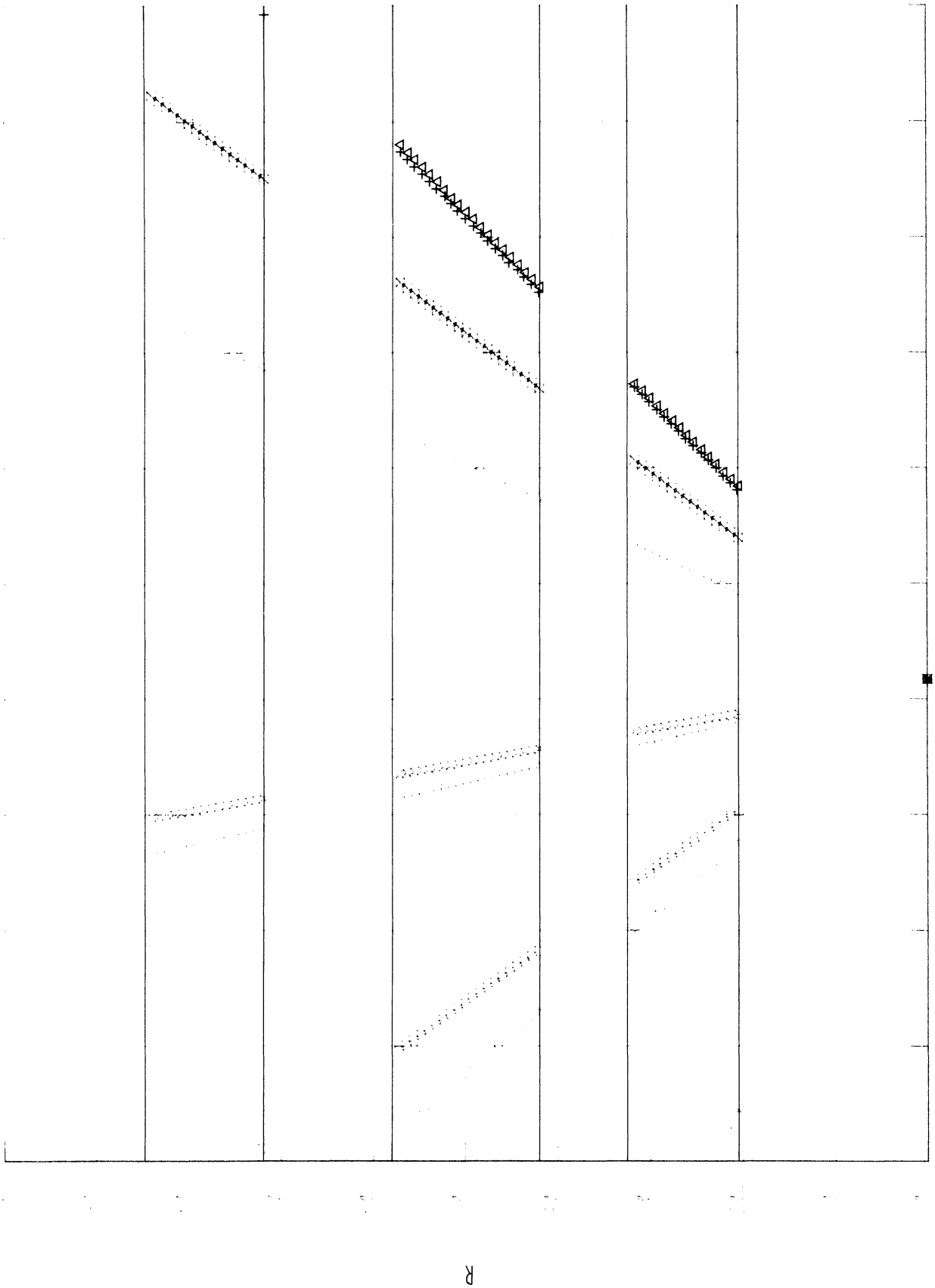

Fig. 10

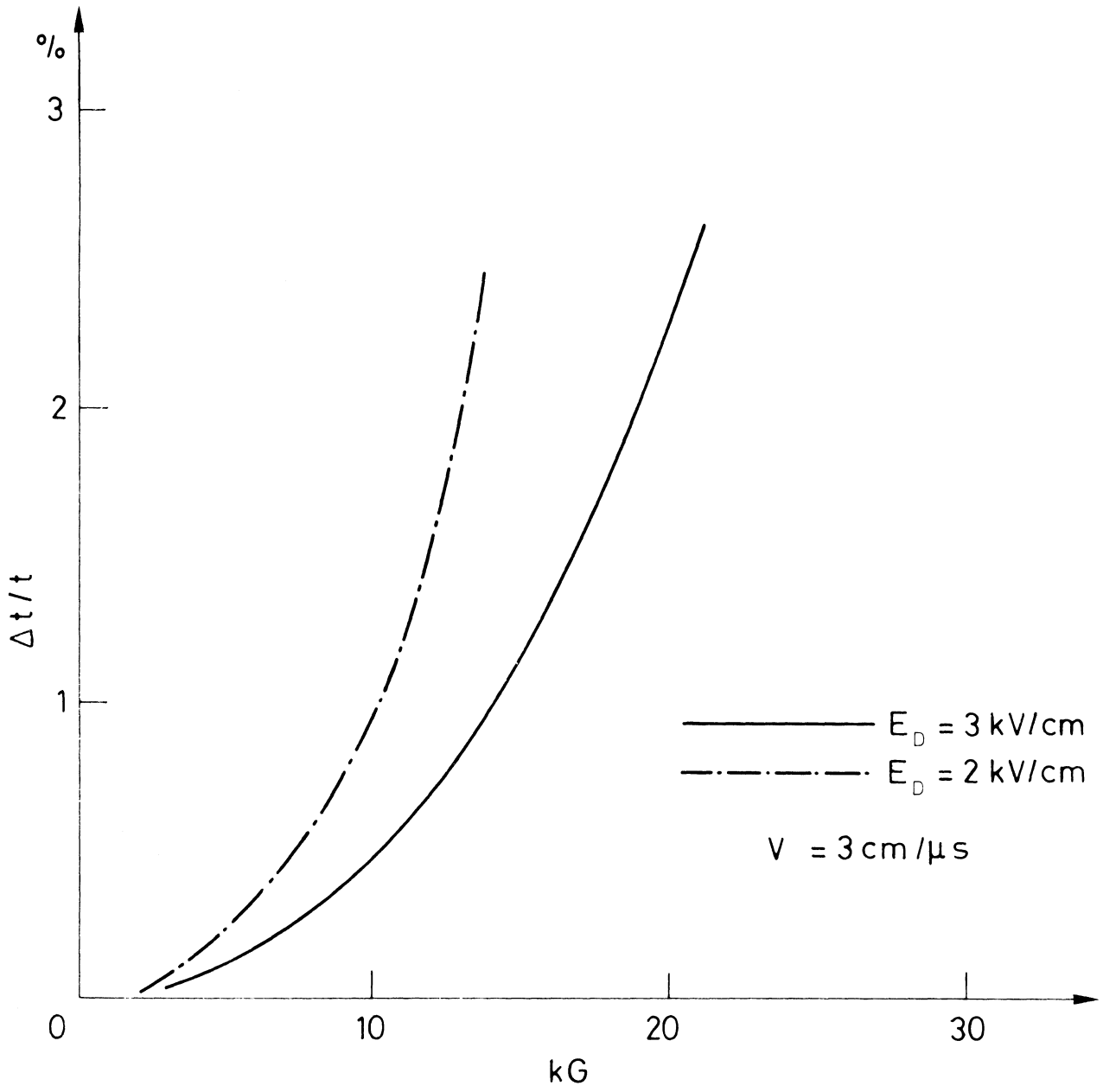

Fig. 11

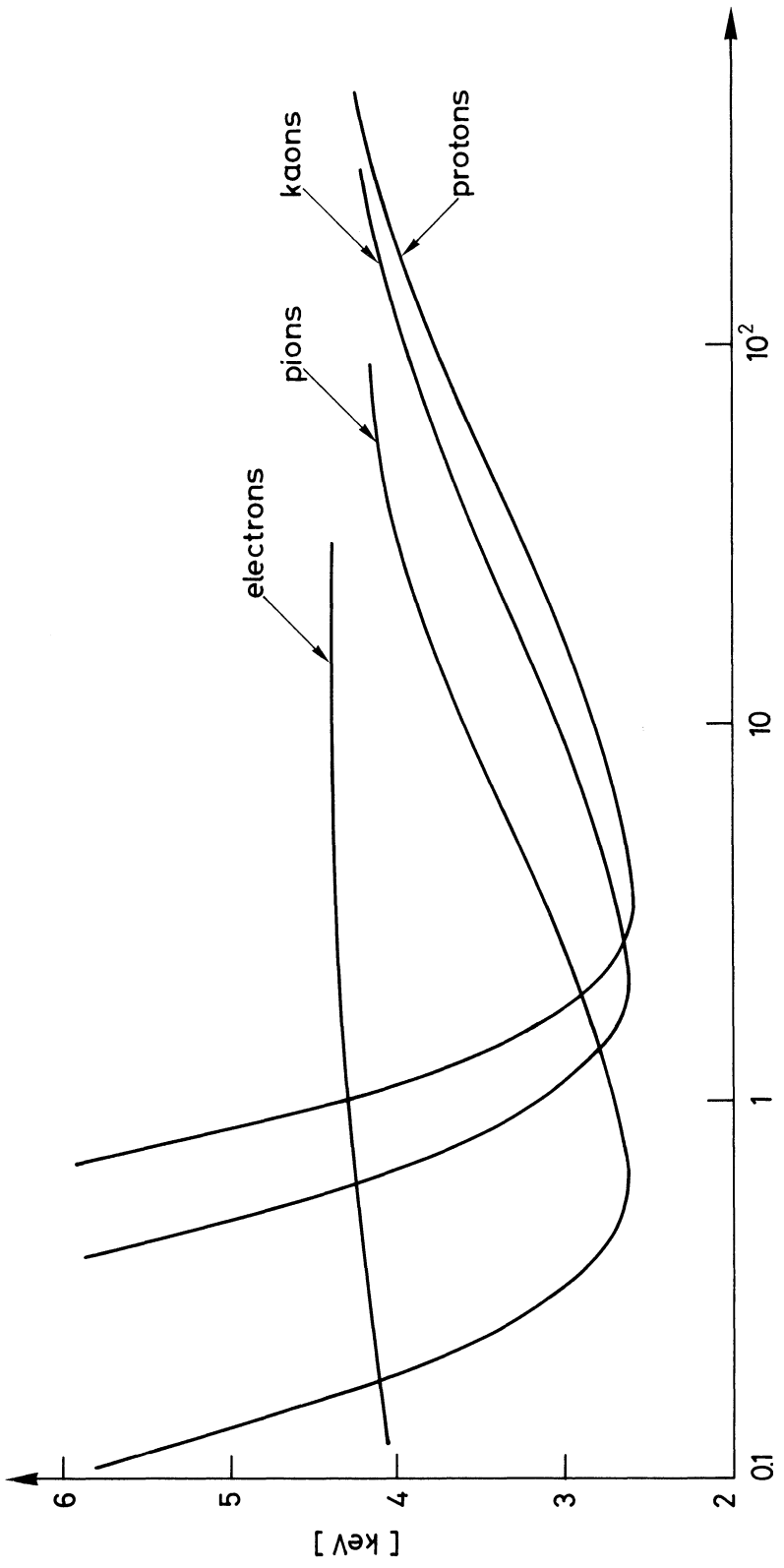

Fig. 12

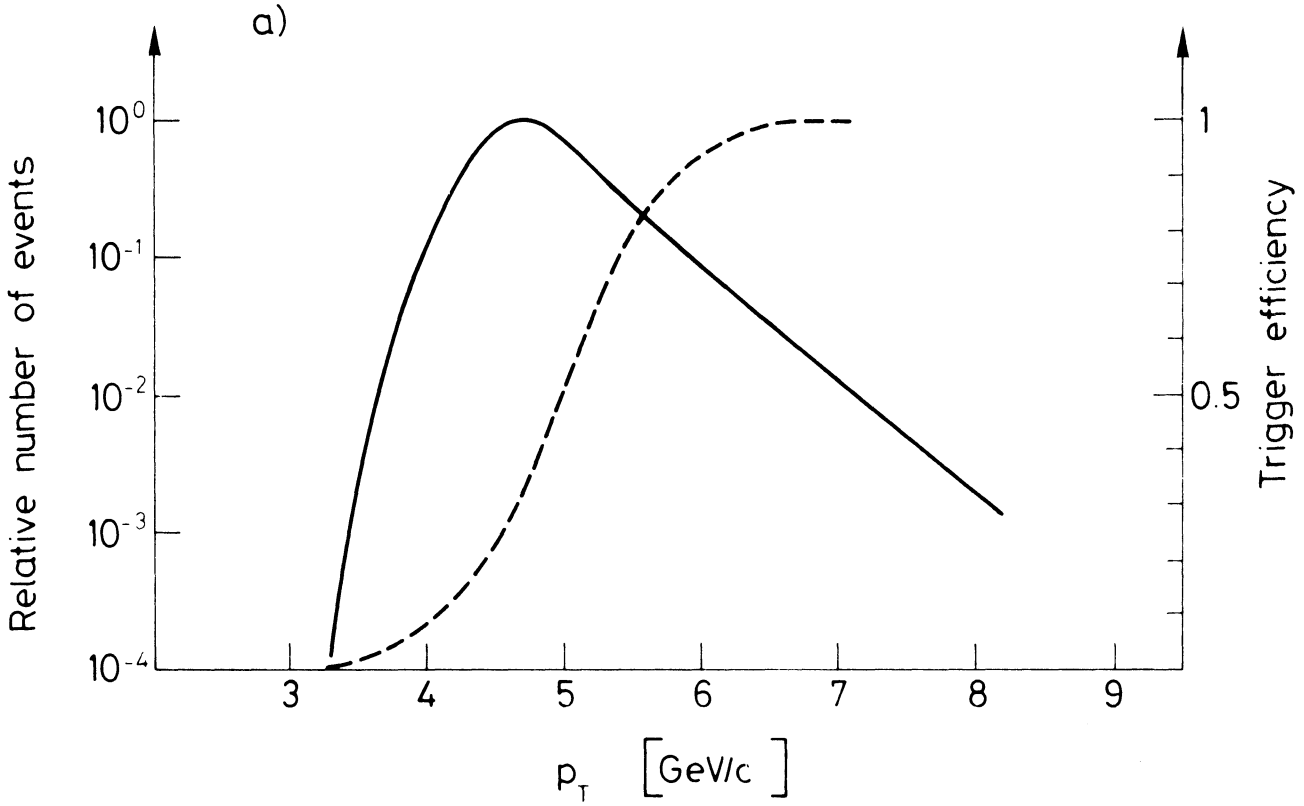
a)
Relative number of events
10^0
10^{-1}
10^{-2}
10^{-3}
10^{-4}
1
0.5
Trigger efficiency
3
4
5
6
7
8
9
p_T [GeV/c]

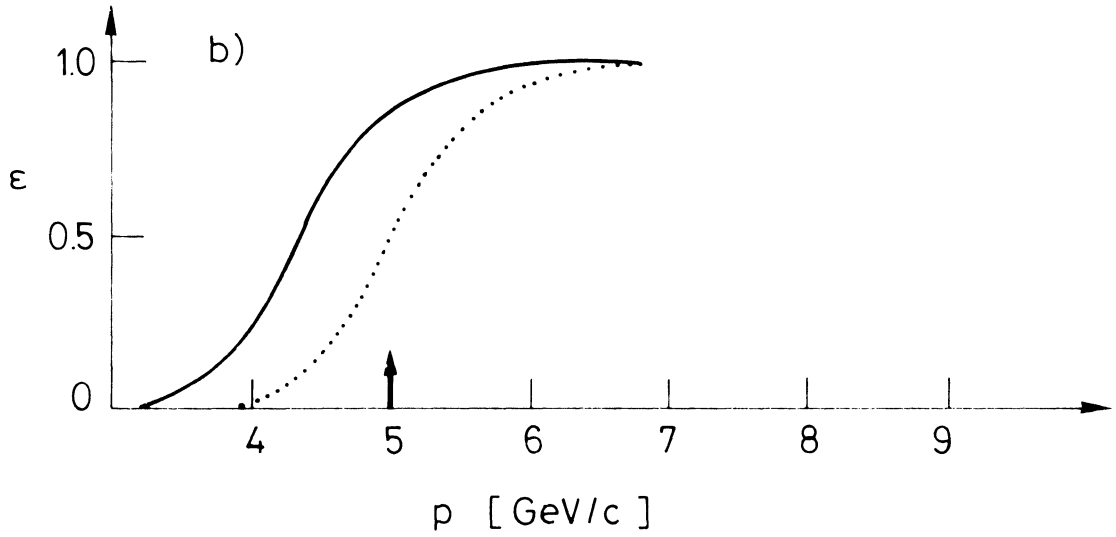
b)
1.0
0.5
0
ε
4
5
6
7
8
9
p [GeV/c]

Fig. 13

APPENDIX

ISR-BOM/TMT/rh
Internal Note

16 December 1976

THE OPEN AXIAL FIELD MAGNET

T.M. Taylor

It is clear that in order to identify particles with large transverse momentum, there are certain advantages in having an axially symmetric magnetic field concentric with the bisector of the incident beams. The most efficient axial field magnet, the solenoid, suffers from the drawback of having its coil in the way of the outgoing particles and of the detectors. The design described here is an attempt to produce an axially symmetric field which is completely open over a very large solid angle, albeit with a modest field. More precisely, the design is a solution to the problem of maximizing the open polar angle about $\theta = 90^{o}$ subject to providing an integrated bending field of ≥ 0.5 Tm along a ray from the centre of the (1.5 m long) gap to a cylinder of radius 1 m, and subject to leaving a suitable passage for the ISR beams.

Description and characteristics of the magnet

The open axial field magnet, which, for speed of manufacture, is of conventional iron yoke and copper coil construction, is shown in Fig. A.1. The magnet consists essentially of two hollow poles, of truncated conical geometry, supported from a large double rectangular frame. The magnetomotive force is provided by circular coils stacked in pancakes around the cones. The total height of the structure is limited by the clearance between the tunnel crane and the plane of the beams. The pole base separation, and hence the total length of the device, is dictated by space requirements for the calorimeter. An opening of $-15^{o} \leq \theta \leq 15^{o}$ is necessary for the passage of the beam pipes through the pole tip.

The basic characteristics of the magnet can be summarized as follows:

- pole tip separation : 1.5 m
- deflecting power : ≥ 0.5 Tm from centre to a cylinder of radius 1 m, $40^{o} < \theta < 140^{o}$
- acceptance, polar : $0 < \theta < 15^{o}$, $40^{o} < \theta < 140^{o}$, $165^{o} < \theta < 180^{o}$
  azimuthal : completely open to a cylinder of radius 2.5 m, then $-60^{o} < \phi < 60^{o}$

- pole base separation : 4.7 m
- overall length : 5.5 m
- overall height : 5.8 m
- overall width : 3.0 m
- total weight of iron : 200 t
- total weight of copper : 10 t
- power dissipation : 1 MW max.

The field shape in this magnet is indicated in Fig. A.2. It is interesting to note that the deflecting power increases as θ goes from 90^{o} to 40^{o} (see Fig. A.3). The radial dependence of field at 90^{o} for various power levels is shown in Fig. A.4.

Assembly

The assembly of the magnet will proceed as follows:

The two lower yokes will first be positioned on the supporting I-beams, and the lower halves of the uprights will be placed on their ends and bolted to the yokes. The upper halves of the uprights will then be lifted into position, and the conical poles with the coils will be placed on temporary supports on the lower yokes, ready to be lifted into position when the frame is complete. These operations will be performed using the 30 t crane. The mobile 4 t crane will then be used to lift into place the plates which form the upper yokes, and these will be bolted to the uprights. The final operation will be to lift the poles, reaching through the gap between the upper yokes with the 30 t crane, and present their bases into the recesses in the uprights, to which they will be bolted.

Compensation

Suitable compensation will have to be provided for this device in order to avoid affecting the ISR beams.

- Radial field component: Since the ISR beams traverse the magnet at 7.5^{o} to the axis, they will experience an integrated radial field of 0.155 Tm. This can be compensated in the same intersection by using two small radial field magnets, 5 m upstream and 6 m downstream of the spectrometer, as shown in Fig. A.5. The vertical position of the beams at the

point of intersection will vary slightly with magnet excitation and beam momentum, but this could eventually be cancelled by using the horizontal field magnets of the machine.

- Coupling: axial fields give rise to coupling between the horizontal and vertical betatron oscillations. By the time this magnet is installed in the ISR, the new skew quadrupole scheme will be in operation, and this will be easily capable of neutralizing the coupling which this device will cause.
- Nonlinear effects: analysis to date indicates that if normal ISR beams pass through the open axial field magnet symmetrically, the integrated nonlinear effects are very small and should not cause variable Q-shifts across the aperture, beam tilt or significant resonance excitation.

Timescale

It is estimated that detailed design, tendering and obtention of all the components will take about 15 months from the time the project is approved, and that assembly, adjustments, tests and magnetic measurements will take another 3 to 4 months. Installation and commissioning in the ISR tunnel will require a 6- to 8-week shutdown.

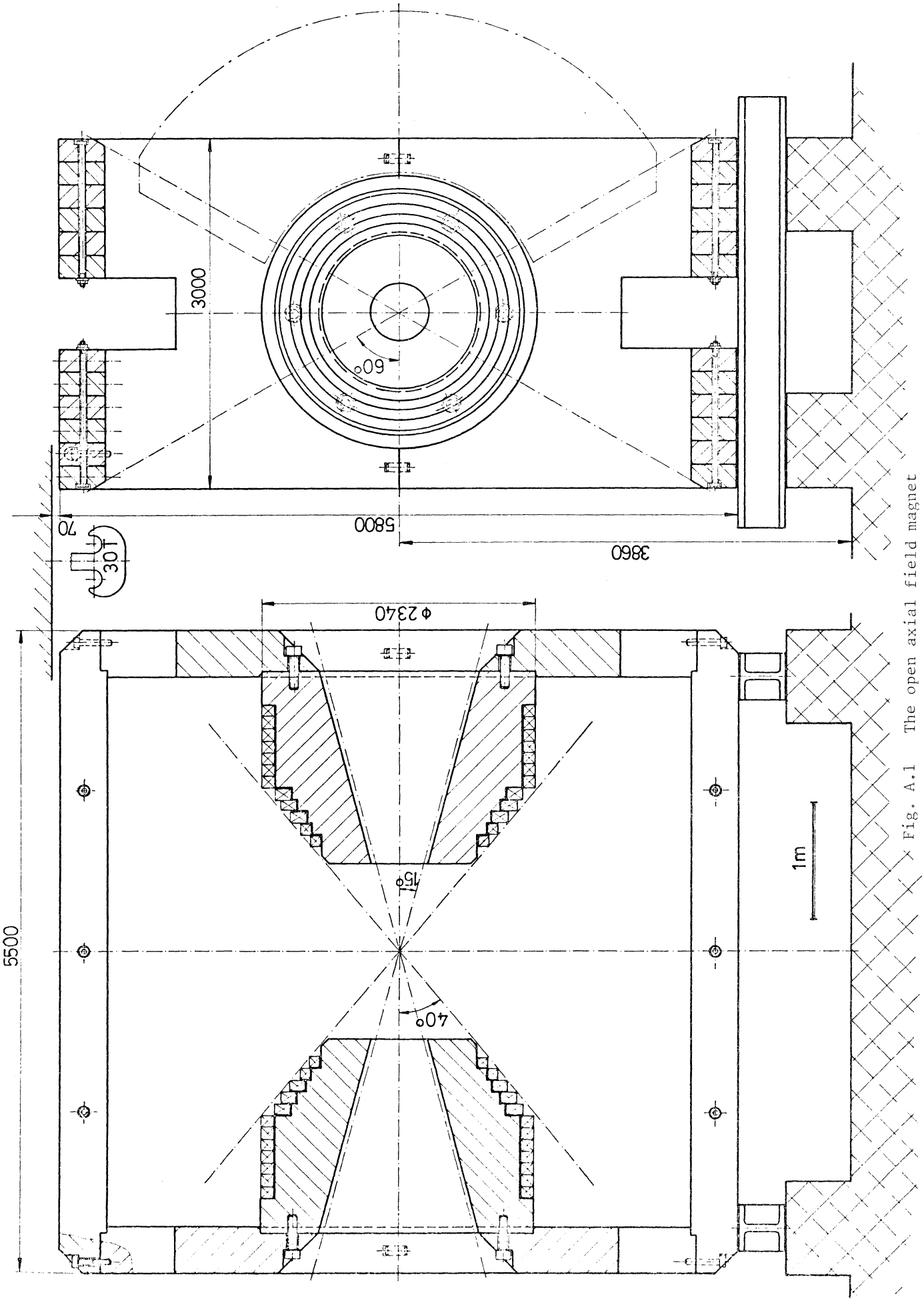

Fig. A.1 The open axial field magnet

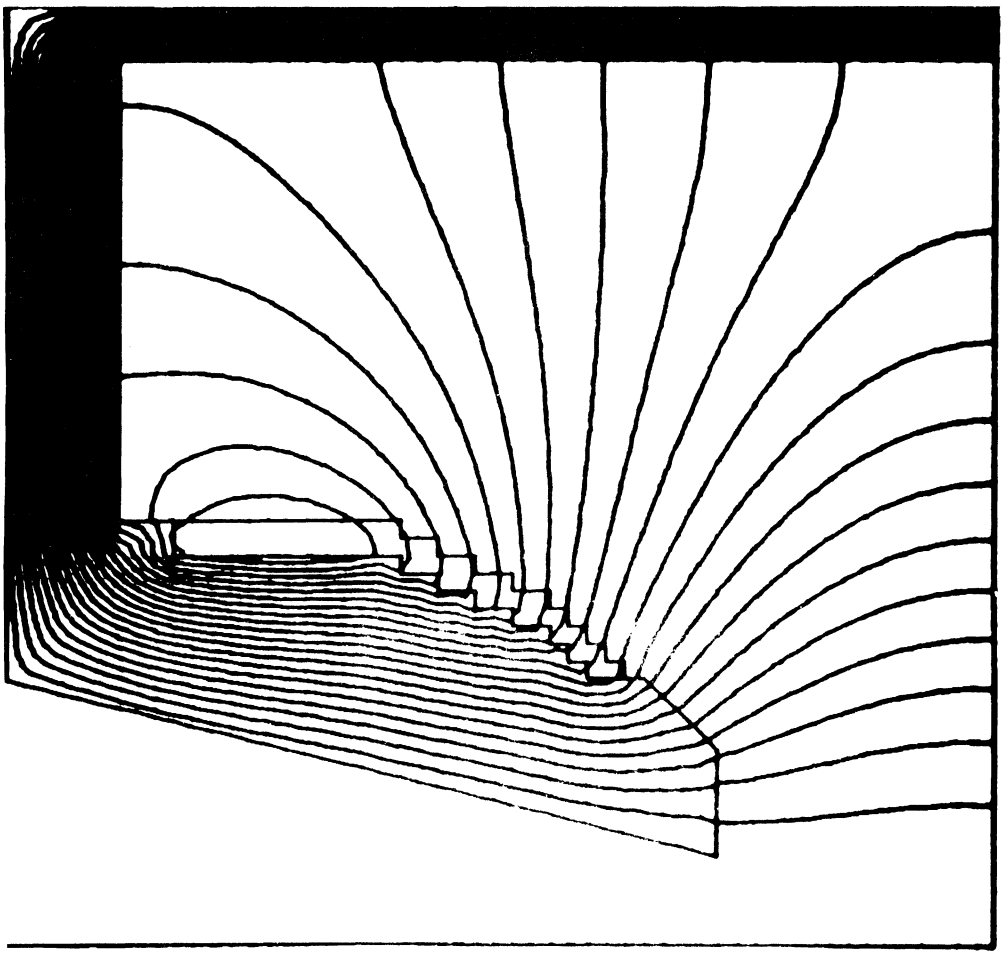

Fig. A.2 Flux lines in the device

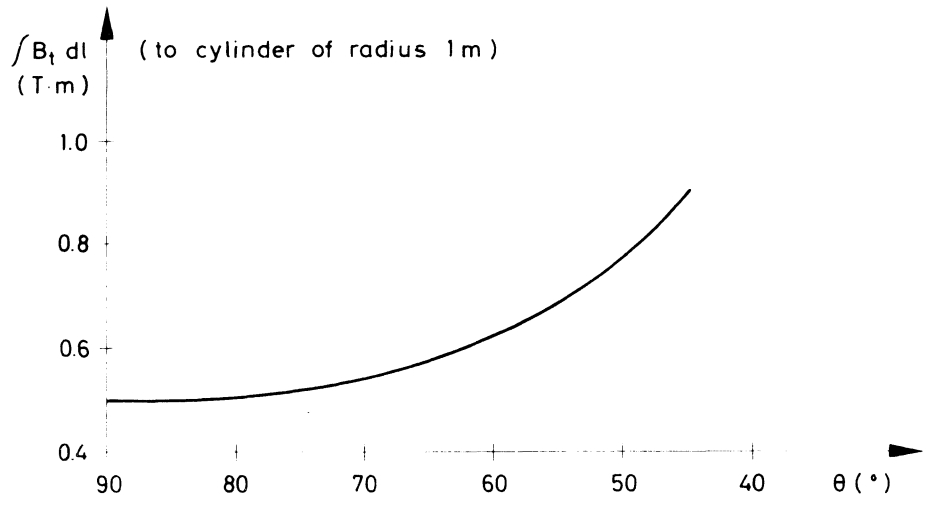

Fig. A.3 Deflecting power as a function of polar angle

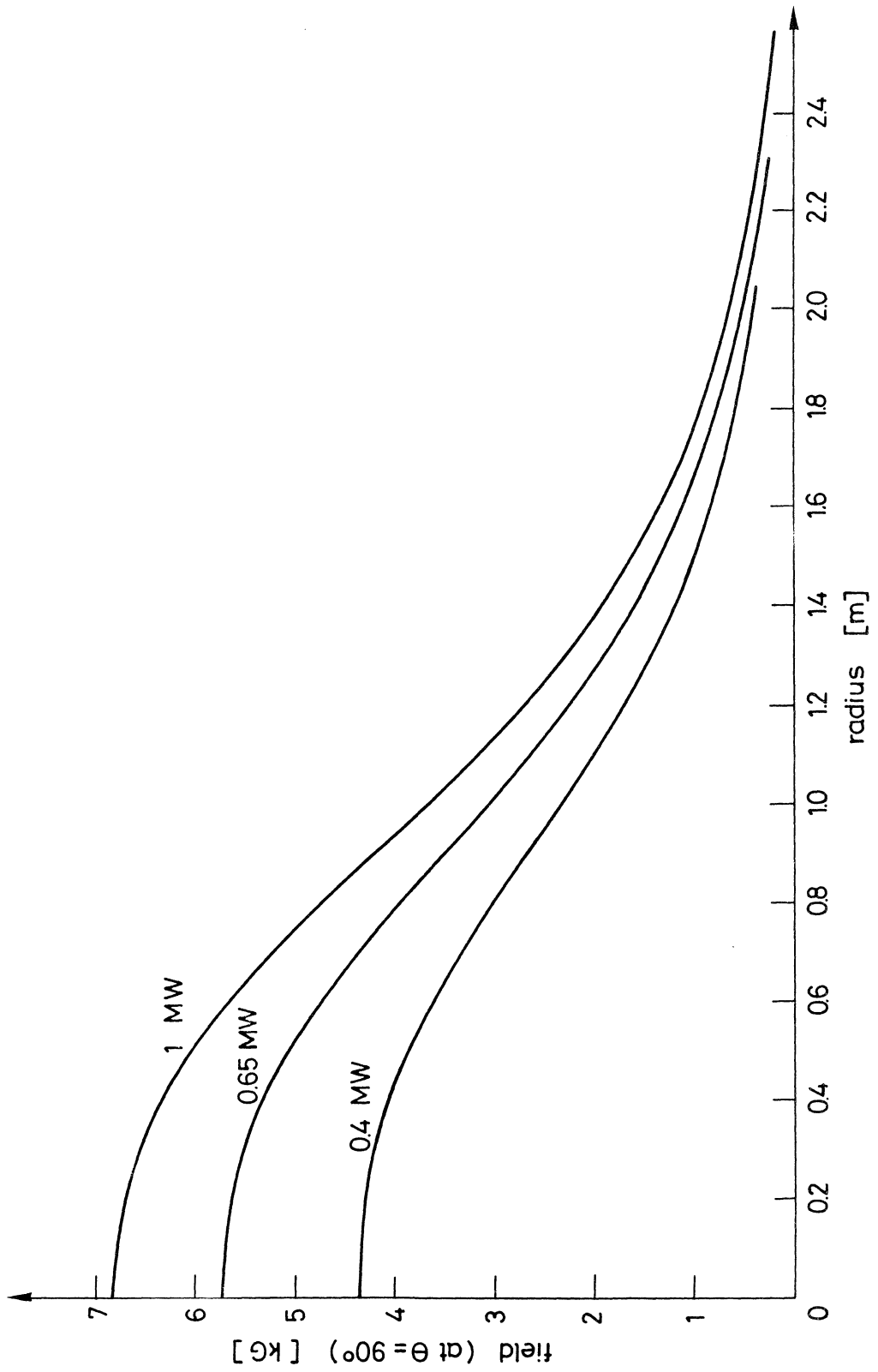

Fig. A.4 Radial dependence of field at 90°

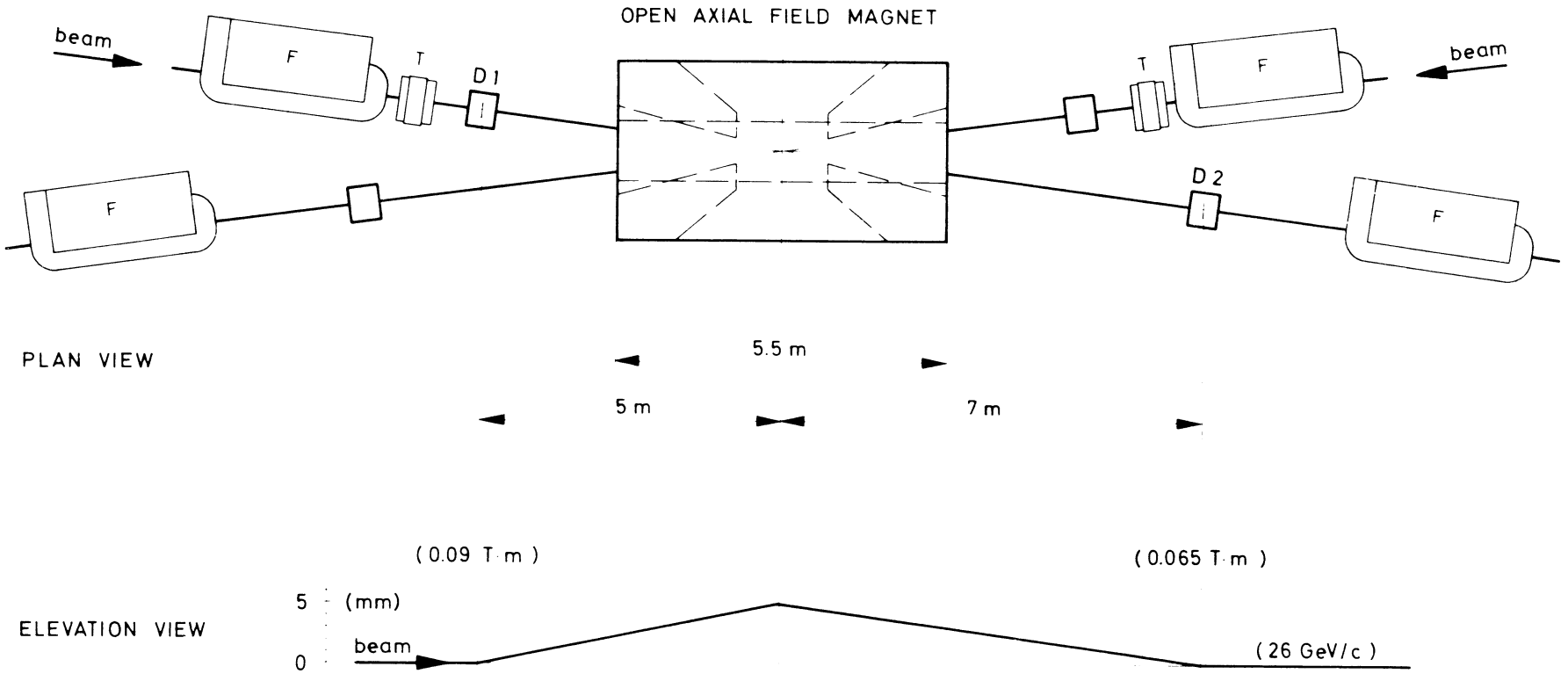

Fig. A.5 Compensation scheme for the radial field component